Journal of Theoretical Biology 265 (2010) 524–534

Contents lists available at ScienceDirect

Journal of Theoretical Biology

journal homepage: www.elsevier.com/locate/yjtbi

Spatiotemporal BOLD dynamics from a poroelastic hemodynamic model

P.M. Drysdale [a,b,*], J.P. Huber [a,b], P.A. Robinson [a,b], K.M. Aquino [a,b]

[a] School of Physics, University of Sydney, NSW 2006, Australia
[b] Brain Dynamics Center, Westmead Millenium Institute, Sydney Medical School - Western, University of Sydney, NSW 2145, Australia

ARTICLE INFO

Article history:
Received 15 February 2010
Received in revised form
13 May 2010
Accepted 20 May 2010
Available online 26 May 2010

Keywords:
Functional MRI
Blood oxygen level dependent
Spatial and temporal dynamics
Porous medium

ABSTRACT

A quantitative theory is developed for the relationship between stimulus and the resulting blood oxygen level dependent (BOLD) functional magnetic resonance imaging (fMRI) signal, including both spatial and temporal dynamics for the first time. The brain tissue is modeled as a porous elastic medium, whose interconnected pores represent the vasculature. The model explicitly incorporates conservation of blood mass, interconversion of oxygenated and deoxygenated hemoglobin, force balance within the blood and of blood pressure with vessel walls, and blood flow modulation due to neuronal activity. In appropriate limits it is shown to reproduce prior Balloon models of hemodynamic response, which do not include spatial variations. The regime of validity of such models is thereby clarified by elucidating their assumptions, and when these break down, for example when voxel sizes become small.

1. Introduction

The purpose of this paper is to develop a model that accounts for both the spatial and temporal dynamics underlying hemodynamic responses that determine the blood oxygen level dependent (BOLD) signal used in functional magnetic resonance imaging (fMRI). Hemodynamic modeling based on physiological processes will also provide new constraints and priors for use in conjunction with empirical BOLD analysis methods. In this paper we thus build a model to explicitly model spatiotemporal BOLD responses. We also clarify how Balloon models emerge as limiting cases of this model.

The BOLD signal is an indirect measure of neuronal activity since a number of physical hemodynamic processes interact to determine the BOLD signal and these processes must be modeled to relate neuronal activity to observed BOLD signals more precisely (Buxton et al., 1998; Friston et al., 2000; Logothetis et al., 2001; Nair, 2005). Moreover, interpretation of BOLD measurements is often impeded by poor signal to noise ratios (e.g., Lund et al., 2005; Long et al., 2005) and by incomplete understanding of the hemodynamics and its coupling with neuronal activity. In this context, improved modeling can provide additional constraints on the dynamics which can be used to improve signal to noise ratios and enable new tests of underlying mechanisms.

Among, the benefits of a spatiotemporal hemodynamic model are that it will allow the derivation of spatiotemporal hemodynamic response functions and allow better understanding of the spatial aspects of hemodynamic response and their links to underlying neural activity. Imposing spatial consistency in building the model also has benefits aside from modeling the spatial dependence of BOLD: because the spatial and temporal aspects of BOLD are intimately connected, it will aid in clarifying the interaction between flow and volume relationships in BOLD, which are still active areas of research (Nair, 2005). Moreover, voxels are becoming smaller with advances in technology, so connections between the hemodynamics of adjacent voxels are likely to become increasingly important, an effect not included in purely temporal models of BOLD response. The present model can assist in understanding such effects, and is thus formulated on a physical basis independent of instrumental factors such as an assumed voxel size.

The Balloon model of Buxton et al. (1998) has been influential in physiological BOLD modeling. Numerous refinements and variations have been made to the original model so that a considerable number of Balloon models have now been proposed (e.g., Buxton et al., 1998; Friston et al., 2003; Mandeville et al., 1999; Kong et al., 2004; Zheng et al., 2005). Balloon models incorporate the common feature that adjacent voxels are hemodynamically independent and each voxel contains one or more vascular "balloons". Consequently, spatial aspects of hemodynamic response are not directly modeled in Balloon models. We note, historically Balloon models consider the

* Corresponding author at: School of Physics, University of Sydney, NSW 2006, Australia.
E-mail addresses: p.drysdale@physics.usyd.edu.au (P.M. Drysdale), p.robinson@physics.usyd.edu.au (P.A. Robinson), aquino@physics.usyd.edu.au (K.M. Aquino).

0022-5193/$ - see front matter © 2010 Elsevier Ltd. All rights reserved.
doi:10.1016/j.jtbi.2010.05.026

mapping between blood flow and observed signal, while hemodynamic models complete Balloon models by pre-pending a model of neurovascular coupling. In this paper we use the terminology Balloon model descriptively rather than categorically so that if the model contains a constituent component which is equivalent to a "balloon" structure we term it a Balloon model. Thus, for example, in this paper the hemodynamic model of Friston et al. (2003) is described a Balloon model since one component of the model includes a "balloon" structure.

In order to model the vasculature in this paper, we use a so called poroelastic approach in which the brain tissue is modeled as an elastic medium with interconnected pores representing the vasculature. Such models are akin to poroelastic models of geophysical fluid dynamics (Wang, 2000). In Section 3, a neuronal signal equation is derived that governs how a change in neural activity leads to a change in flow. The relationship between blood flow and blood volume, as governed by conservation of blood mass, is then derived in Section 4. The blood deoxygenation process, which conserves hemoglobin while describing the conversion of oxygenated to deoxygenated hemoglobin, is governed by an equation derived in Section 5. A force balance equation which describes the interaction between blood vessel walls and the blood, and the internal pressures within the blood is then derived in Section 6. Section 7 recasts a recently published relation between BOLD signal, blood volume and deoxygenation for use in the present model. Section 8 discusses the boundary conditions for the model. Section 9 demonstrates that the present model reproduces the Friston et al. (2003) Balloon model as a limiting case. This clarifies the conditions of validity of this and similar Balloon models and immediately implies that the present model can reproduce at least the range of phenomena explained by such Balloon models to date, including the main temporal features of the hemodynamic response and BOLD signal.

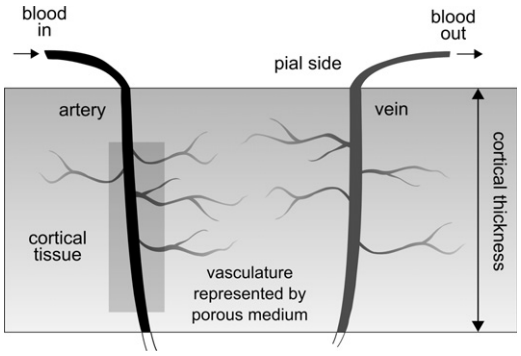

Fig. 1. Schematic cross-section of the cortical gray matter showing approximately vertical descending arteries and ascending veins. The arterioles, capillaries, and venules form a dense network connecting these vessels. The shaded rectangle highlights the blood inflow region which is examined in more detail in Section 8.

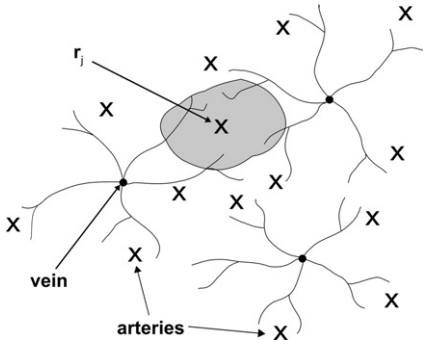

Fig. 2. Schematic view from the pial side of descending intracortical arteries and ascending intracortical veins. Descending arteries (crosses) are positioned around ascending veins (dots) with arteries outnumbering veins approximately 5 or 10–1 (Duvernoy and Vannson, 1981). Lateral branches connecting to ascending veins are shown. One flow regulation site r_j is marked and the approximate area of neural connectivity to that site is shaded.

2. Overview of model

In this paper we develop a 2D spatiotemporal poroelastic model of hemodynamic response. Poroelastic models were originally introduced in geophysics for fluid flow in porous materials (Wang, 2000). Currently the descending and ascending vessels of the vasculature are not fully resolved by fMRI studies as the vessels are significantly finer than the voxel size. The fine structure of the interconnecting vessels can only be resolved by invasive means. Consequently, in order to model the vasculature, we approximate the tissue as a porous elastic medium in which the vessels are represented as "pores" of the medium. We justify this approach with reference to Figures 26–29 of Duvernoy and Vannson (1981), which show cross-sectional slices through the cortex, including ascending and descending vessels and the vasculature between. This structure is schematically represented in Fig. 1, which does not show the full density of connecting vessels. From anatomical studies (Duvernoy and Vannson, 1981) it is known large vessels are located on the outer surface of the cortex, then intracortical arteries descend into cortex, and are connected via arterioles, capillaries, and venules to intracortical veins ascending back to the surface, as shown schematically in Fig. 1. When viewed from above, a star-like formation of input and output points can be seen as in Fig. 2 (adapted from Fig. 61 of Duvernoy and Vannson, 1981). In view of the extreme density and fineness of the actual vascular network connecting the intracortical arteries and veins, we thus approximate this network as a set of interconnected pores in an elastic matrix.

Before proceeding it is important to clarify how tissue properties are averaged over different types of vasculature. Specifically, our model is a *one-compartment* model in which we model the weighted averaged properties of the arterioles, capillaries, venules, and intra-gray matter venous vessels. Single compartment Balloon models are common and able to approximate the major features of the temporal response. Multi-compartment Balloon models have been proposed to account for fine structure of temporal response (e.g., Zheng et al., 2005; Mandeville et al., 1999) and experimental measures of the relative differences between the hemodynamics of different compartments is described by Vanzetta et al. (2005). Within multi-compartment models the different vascular components arterioles, capillaries etc. are separated into one or more averaged components yielding improved modelling of temporal response. It should be noted that though each distinct type of vasculature necessarily occupies distinct spatial locations though this is not directly related to the spatial dimensions considered in the present model which represent spatial dimensions on the cortical sheet. It is beyond the scope of the present paper to model the vascular compartments separately, although such a refinement could be added in the future.

The cortical sheet has a layered structure with the anatomy of the vasculature differing between layers, while the layers themselves are comparatively very similar across the cortex. It is unclear from anatomical studies whether input blood flow is separately regulated as it passes between the cortical layers (Smirnakis et al., 2007). Experimental results of Smirnakis et al. (2007) suggest that BOLD is unlikely to have interlayer specificity, whereas Shmuel et al. (2006) showed increased BOLD response near layers 4 and 5. It is possible that the increased BOLD

response near layers 4 and 5 may be due to variation in vascular density (Shmuel et al., 2006) rather than flow regulation between layers, consistent with the findings of Smirnakis et al. (2007). For these reasons, this paper implements a 2D spatial model, which aggregates over the cortical depth, rather than a 3D model; more detailed anatomical studies and/or clearer interlayer BOLD measurements would motivate future modeling of the spatial dependence of the BOLD response versus cortical depth.

A number of physical processes are included in our poroelastic model and their interactions are shown in Fig. 3. These are that: (i) a change in neural activity causes a change in blood inflow; (ii) the change in blood inflow leads to changes in the cerebral blood volume; (iii) simultaneously, deoxygenation of the blood in the capillaries leads to variation in the dHB content of the blood; and (iv) the relative changes in blood volume and dHB content contribute to changes in the detected BOLD signal. The model thus involves four primary governing equations, one for each of these processes. There is also an equation that relates the observed BOLD signal to the underlying hemodynamic quantities.

Balloon models have been successful in accounting for the main aspects of temporal BOLD response (Buxton et al., 1998; Mandeville et al., 1999; Kong et al., 2004). We show our spatiotemporal model reproduces a Balloon model in a certain limit, thereby clarifying the conditions for validity of Balloon models. By reproducing a Balloon model, in the appropriate limit the present model can reproduce at least the range of phenomena explained by that model. Since our main aim is to model spatial BOLD we do not exhaustively survey the various refinements to Balloon models that have been proposed in the literature, although some are mentioned at relevant points.

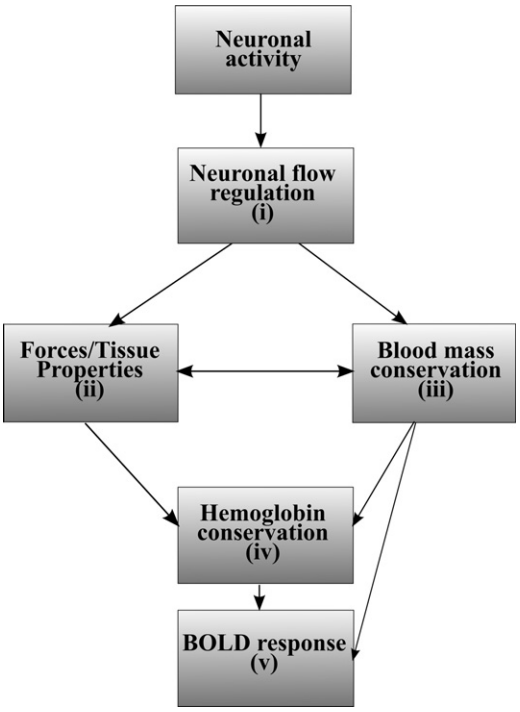

Fig. 3. Block diagram showing the major physical processes modeled in the poroelastic model. Neuronal activity causes (i) changes in flow regulation via neuronal signal equation, (ii) forces between blood and tissue and within the blood are governed by a force balance equation, (iii) blood flows are governed by blood mass conservation equation, (iv) deoxygenation of blood governed by hemoglobin conservation equation, and (v) generation of BOLD signal response occurs via changes in blood volume and deoxygenation as described by a BOLD signal equation. The arrows mark components of the model that depend on the same physical quantities. The direction of the arrows represents causal links in these physical quantities.

3. Coupling of neuronal activity and blood flow

In this section an equation is derived to describe how a change in neuronal activity causes a change in blood inflow. The details of this coupling are not fully understood and constitute an area of active research (Reira et al., 2006; Bennett et al., 2007). However, it is widely agreed that astrocytes mediate the signal from neurons that causes dilation of arterioles and a resulting increase in blood flow (Zonta et al., 2003; Haydon and Carmignoto, 2006); hence, we model this link at this level.

In developing a spatial model it is necessary to determine where the blood flow control occurs. Duvernoy and Vannson (1981) suggested flow control of blood inflow into the cortex was in arteriole zone and sphincter-like constrictions on arterioles might operate as the flow control points. The constrictions Duvernoy and Vannson (1981) observed were at the limits of resolvability but Harrison et al. (2002) resolved sphincter muscles on arterioles and vascular pericytes near capillary junctions with arterioles and identified them as sites of blood inflow control. Our 2D spatial model does not depend critically on the exact site of flow control, except that it is assumed to be located within the cortex in an arteriole inflow zone; for definiteness we assume it to lie near descending arteries, as argued by Harrison et al. (2002).

In order to model the spatial dependence of the coupling of neural activity to flow we note that a signal requiring the change in flow caused by the activity of neurons must propagate from the neurons to the regulation/constriction sites on the blood vessels. This signal is believed to be originated by astrocytes (Zonta et al., 2003), probably by activation of glutamatergic (AMPA) receptors. These cells then generate a vaso-dilatory signal (nitric oxide or NO), which diffuses rapidly and locally to act as an endothelium relaxing factor and increase blood flow. In the present model we neglect the time delay for this propagation relative to the time scales of the other physical processes.

The temporal dynamics of the regulation of flow control must be modeled. Experiments have measured flow control response to sudden changes in neuronal activity via MRI, optical, and ultrasound Doppler methods. For modeling purposes it is important to know whether the flow can undershoot its equilibrium value after a sudden fall in neuronal activity. Conrad and Klingelhöfer (1989) observed flow undershoot using ultrasound Doppler measurement. The results of Conrad and Klingelhöfer (1989) are particularly persuasive since ultrasound Doppler measurement is preferentially sensitive to the largest flow velocities and so is less contaminated by flow velocity further down the vascular tree. In light of the experimental evidence for flow undershoot we generalize the temporal flow control mechanism introduced by Friston et al. (2003) to account for spatially regulated flow control. Friston et al. (2003) modeled the flow control as having dynamics analogous to a damped harmonic oscillator (DHO), thus incorporating a flow undershoot (Robinson et al., 2006).

For a particular regulation site $\mathbf{r}_j$ the flow control in the present model is given by

$$\frac{d^2F(\mathbf{r}_j,t)}{dt^2}+\kappa\frac{dF(\mathbf{r}_j,t)}{dt}+\gamma[F(\mathbf{r}_j,t)-F_0]=\int h(z,\mathbf{r}-\mathbf{r}_j)\,d\mathbf{r}, \tag{1}$$

where F is the flow, κ is the flow signal decay rate (i.e., the rate at which signal decreases after neural activity ceases.), γ is the flow-dependent elimination constant ($\sqrt{\gamma}$ is the inverse of the characteristic time for autoregulatory feedback from blood flow). The quantity $h[z(\mathbf{r}-\mathbf{r}_j)]$ is a weight function that reflects the contribution of neural activity z from $\mathbf{r}$ to driving flow regulation at $\mathbf{r}_j$. This function falls off over a nonzero characteristic range that

reflects the finite range of astrocytic projections (Zonta et al., 2003; Haydon and Carmignoto, 2006).

A number of aspects of Eq. (1) merit further discussion:

(i) The distribution $h[z(\mathbf{r}-\mathbf{r}_j)]$ of effective connectivity between neurons and flow regulation points has not been measured experimentally but is an area of significant research interest. Models of this effective connectivity have been proposed (see e.g. Friston, 1995). The incorporation of such a model is a possible future refinement of the present model.

(ii) Nair (2005) reviewed the uncertainty and disagreement in the literature as to whether a flow undershoot is of significance in generating observed undershoots in BOLD response. In modeling the coupling of neural activity to flow control our aim is to accurately characterize the flow control in this component of the model. Although we include the possibility of an undershoot in flow (which would correspond to small κ), we do not examine its role in generating BOLD undershoots here.

(iii) On the left hand side of Eq. (1) the final term is $\gamma(F-F_0)$ where F_0 is the equilibrium flow. Thus the oscillation of the flow is about this equilibrium value. The form of this term was proposed and explained by Friston et al. (2000) and motivated by slow fluctuations observed in fMRI and optical imaging. It should be noted that our equilibrium flow is a dimensional quantity in contrast to the normalized equilibrium flow of Friston et al. (2003). Recently numerous studies have considered what have been termed "resting" or "default" networks, in which it has been shown that there is fluctuating activity even in what has been termed the "resting brain" (e.g., Raichle et al., 2001; Fox and Raichle, 2007; Damoiseaux et al., 2006). Building a model which incorporates a equilibrium flow is not inconsistent with such studies. since we impose no requirement that prestimulus flow be at the equilibrium level. Indeed it is likely that flow never remains exactly at equilibrium, rather it is constantly perturbed about this value due to ever present fluctuating neural drives arising from the continual flow of external stimuli and, probably, self-generated neural activity.

4. Mass conservation of cerebral blood flow

In this section we derive a governing equation of our poroelastic model that incorporates the physical constraint that blood mass must be conserved. Mass conservation of blood requires that for any volume element of brain tissue the net flux of blood through its boundaries must be balanced by changes in the amount of blood stored within its pores, as shown in Fig. 4. Mathematically this can be expressed for an arbitrary volume element V_v as

$$\frac{dM_V}{dt} = -\int_{\partial V} \rho_f \mathbf{v}\cdot d\mathbf{A}, \tag{2}$$

where M_V is the mass of blood within the volume element, ρ_f the density of blood, and $\mathbf{v}$ the blood velocity and ∂V_v is the surface of V_v. In this case the change in blood storage is represented by the left hand side, while the right hand side expresses the flux of blood into V_v. We define the blood mass content per unit volume ξ to be

$$\xi = \frac{\rho_f V_f}{V_v} = \frac{M_V}{V_v}, \tag{3}$$

where V_f is the blood volume, ρ_f is the density of blood, and V_v is the volume of the volume element. Applying Gauss's divergence theorem and using Eq. (3) yields

$$\frac{d(V_v\xi)}{dt} = -\int_{V_v} \rho_f \nabla\cdot\mathbf{v}\, dV. \tag{4}$$

Eq. (4) can be converted to differential form (Griffiths, 1989), yielding

$$\frac{\partial\xi(\mathbf{r},t)}{\partial t} = -\rho_f \nabla\cdot\mathbf{v}(\mathbf{r},t), \tag{5}$$

where we have restored the arguments $\mathbf{r}$ and t for clarity. In this form, the left hand side expresses the change in fractional blood storage in the pores while the right hand side expresses the net flux inward of blood per unit volume.

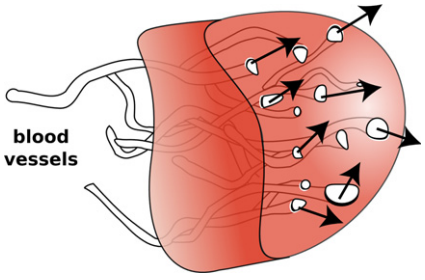

Fig. 4. Schematic showing inflow and outflow of blood through pores in an arbitrary 3D volume element. Differences between inflow and outflow are balanced by changes in blood storage within the volume element. Direction of blood flow is marked with arrows.

5. Conservation of hemoglobin

In this section we derive an equation to describe the spatiotemporal evolution of deoxyhemoglobin (dHB) concentration. This equation can be derived from hemoglobin conservation since, analogously to blood mass, hemoglobin is conserved when input and output flows are accounted for. The conserved total hemoglobin (HB) is the sum of oxygenated hemoglobin (oHB) and dHB components. Neither oHB or dHB is separately conserved because the metabolic demands of the tissue convert oHB to dHB. Conservation requires

$$Q(\mathbf{r},t)+C(\mathbf{r},t) = B(\mathbf{r},t), \tag{6}$$

where $Q(\mathbf{r},t)$ is the local concentration of unoccupied oxygen sites on hemoglobin molecules in erythrocytes in the blood, $C(\mathbf{r},t)$ is the local concentration of occupied oxygen sites on hemoglobin molecules in erythrocytes in the blood, and $B(\mathbf{r},t)$ is the total local concentration of oxygen sites, both occupied and unoccupied, on erythrocytes. Further, $B(\mathbf{r},t)$ can be written as $B(\mathbf{r},t)=\xi(\mathbf{r},t)\psi$, where ψ is the concentration of oxygen sites per unit mass of blood and ξ is the fractional blood mass content defined in Section 4. The conservation relation (6) then becomes

$$Q(\mathbf{r},t)+C(\mathbf{r},t) = \xi(\mathbf{r},t)\psi. \tag{7}$$

The conversion of oHB to dHB can be modeled by considering the oxygen dissociation curve (ODC), which relates the oxygen saturation of HB to the partial pressure of dissolved oxygen in the blood (Hoffbrand et al., 2004). The ODC is approximately linear for the partial pressures of dissolved oxygen typical in capillaries and veins (Hoffbrand et al., 2004). Further, assuming that diffusion is passive between oxygen dissolved in the blood and the surrounding tissue the rate of conversion of oHB to dHB can be approximated as being proportional to oHB concentration. The conversion of oHB to dHB is then given by

$$\frac{dQ_{o\to d}(\{\mathbf{r},t\})}{dt} = \eta C(\mathbf{r},t) \tag{8}$$

$$= \eta[\xi(\mathbf{r},t)\psi - Q(\mathbf{r},t)], \tag{9}$$

where η is the fractional rate of oxygen consumption. By analogy with mass conservation, the total change in dHB sites in a volume element is equal to the sum of the net inward flux dHB sites and the rate of production of dHB sites within the element via deoxygenation; i.e.,

$$\int_V \frac{\partial Q}{\partial t}\, dV = -\int_{\partial V} Q\mathbf{v}\cdot d\mathbf{A} + \int_V \eta(\xi\psi - Q)\, dV, \tag{10}$$

where the term on the left hand side represents total rate of change in deoxyhemoglobin content, the first term on the right hand side (including the minus sign) represents the flow rate of deoxyhemoglobin into the volume element and the second term incorporates the rate of production of deoxyhemoglobin via deoxygenation. Applying Gauss's divergence theorem and converting to differential form (Griffiths, 1989) then yields

$$\frac{\partial Q}{\partial t} = -\nabla\cdot(Q\mathbf{v}) + (\psi\xi - Q)\eta. \tag{11}$$

This equation expresses the conservation of hemoglobin. In fluid dynamics and classical mechanics literature it is customary to express equations of this type in a more familiar form in terms of the material derivative (Acheson, 1990). The material derivative is a derivative taken with the underlying flow and formally defined by

$$\frac{DA}{Dt} \equiv \frac{\partial A}{\partial t} + \mathbf{v}\cdot\nabla A. \tag{12}$$

To re-express Eq. (11) in terms of the material derivative of Q, the vector identity $\nabla\cdot(f\mathbf{A}) = f(\nabla\cdot\mathbf{A}) + \mathbf{A}\cdot(\nabla f)$ is applied to the first term on the right hand side (Griffiths, 1989), and the chain rule of differentiation is used to give

$$\frac{DQ}{Dt} = -Q\nabla\cdot\mathbf{v} + (\psi\xi - Q)\eta. \tag{13}$$

This equation is analogous to the mass conservation Eq. (5) but includes the source term $(\psi\xi - Q)\eta$, where $(\psi\xi - Q)$ is the concentration of oxygenated hemoglobin and η is the fractional oxygen consumption rate.

Further refinements to the deoxygenation modeling could easily be implemented in this framework. For example, experiments by Vanzetta et al. (2005) are suggestive that deoxygenation may be an active process rather than acting by passive diffusion resulting from the gradient in oxygenation between vasculature and tissue. An active diffusion process could be implemented in this model by making η depend on neuronal activity.

6. Forces between blood and brain matrix and within the blood

In order to describe the dilation of blood vessels due to blood pressure the force balances within the blood and between blood and brain tissue must be modeled. This section derives the force balance condition. In the poroelastic literature (Wang, 2000), force balance relationships are typically obtained by analyzing momentum conservation and we follow this approach here.

We first review experimental understanding of the mechanical properties of the skull contents. The skull contents include the brain and cerebral spinal fluid (CSF), both of which are extremely incompressible due to their high water content. In neurology, the incompressibility of skull contents is known as the Monro–Kellie Principle (Barash et al., 2009). It might naively be expected that increasing cerebral blood volume would introduce enormous pressures and stresses in the brain since relatively incompressible tissue could not otherwise accommodate the increasing cerebral blood volume. However, the incompressibility of skull contents is likely not as significant a problem as it first appears since the Monro–Kellie Principle also states there is some compliance (predominantly via elasticity of some tissues surrounding the spinal compartment) to accommodate small volume changes in the skull contents. Consistent with this, there has been no experimental observation of rises in internal pressures in normal brain tissue due to neurally induced hemodynamics (e.g. Turner and Thomas, 2006).

In the present model any hemodynamically induced increase in pressure is accommodated via the brain tissue moving within the CSF to redistribute any stresses. The redistribution of stresses via pressure coupling between brain tissue and CSF is likely to be very efficient due to similar incompressibility of both media. Any pressure waves in the CSF will be transmitted away at the speed of sound ($\approx 1500\,\mathrm{m\,s^{-1}}$) to where small volume changes (e.g., due to net expansion of brain tissue whose blood content has increased) can be accommodated in the surrounds of the spinal tissue. The brain tissue also has a low shear modulus (due to its high water content) so shear stresses are rapidly accommodated. As the present model is 2D we do not explicitly model the mechanical boundary between brain tissue and CSF, and instead assume that stresses are accommodated via the above mechanism. Thus the model presented here transmits forces via pressure only and is a so called uncoupled poroelastic model (Bear, 1972), in contrast with poroelastic models of other biological tissues described in Fung (1993) where significant stresses are transmitted through solid tissues.

As described above, the model is assumed an uncoupled poroelastic model so that it is unnecessary to introduce a stress tensor to describe the bulk brain matrix. In this case the blood acceleration $\partial\mathbf{v}/\partial t$ is proportional to the sum of the blood pressure gradient and a viscous resistance term; i.e.,

$$\rho_f \frac{\partial \mathbf{v}}{\partial t} = -\left(c_1\nabla P + \frac{\mu\phi}{\kappa}\mathbf{v}\right), \tag{14}$$

where μ is the dynamic viscosity of blood, ϕ is the tissue porosity and κ is the permeability of the tissue. Eq. (14) is known as a *momentum evolution equation* (Wang, 2000). Eq. (14) is derived from the Navier–Stokes equation by assuming a viscous resistance term analogous to the one that yields Darcy's Law (Darcy, 1856; Bear, 1972). Further insight into Eq. (14) can be gained by comparison of this equation with unsteady Poiseuille flow which was originally derived as an approximation of blood flow in a single vessel (Poiseuille, 1846; Acheson, 1990; Bear, 1972). Eq. (14) has the same functional form as aggregated (over many vessels) unsteady Poiseuille flows and thus can be interpreted as a momentum evolution equation describing an aggregate of blood vessels.

In addition to a momentum evolution equation, modeling force balance requires a relationship between pore volume and blood pressure—a *constituent equation* (Wang, 2000). The simplest possible constituent equation is the linear or Hookean elastic type where pore pressure and fluid volume are linearly related. However, for hemodynamic modeling a more complex constituent relationship is required, with

$$P = c_2\xi^{\beta}, \tag{15}$$

where $\beta < 1$ is termed the hyperelasticity coefficient ($\beta = 1$ is the Hookean case) and c_2 is a proportionality constant. A constituent relationship is termed hyperelastic if doubling the pore pressure causes more than a doubling in fluid volume (Fung, 1993). Although *in situ* verification is very difficult, *ex situ* measures of vessels demonstrate that larger blood vessels, especially veins, are hyperelastic (Fung, 1993). Such measures may overestimate *in vivo* hyperelasticity as they neglect the opposing effects of the tissue around the vessels (Fung, 1993), although in brain tissue we argue that these effects are small. In our model we

follow the traditional convention of measuring blood pressure relative to atmospheric pressure.

We note that our assumptions on stresses confine our force balance modeling to cases where intracranial pressure is not already elevated or cerebrospinal compliance is not compromised. For example, the administration of halothane anesthetic has been known to induce hemodynamic changes in CBF sufficient to cause rises in intracranial pressure outside clinical guidelines. This has been an issue when considering halothane as anesthetic for patients where cerebrospinal compliance may be limited (Barash et al., 2009).

In Section 9 we show that $\beta = 1/\alpha$ where α is termed Grubb's constant (Grubb et al., 1974). Mandeville et al. (1999) recognized that for some MRI purposes a time dependence of α can also be important, yielding "delayed compliance". Delayed compliance is the property wherein, after a sudden pressure increase, a vessel continues to expand for some time after the pressure leveled off, due to relaxation of the vessel wall structure. For simplicity, we do not incorporate delayed compliance in the present work, although it could be included by dividing ξ in Eq. (15) by a time dependent compliance parameter in a manner analogous to Kong et al. (2004).

7. BOLD signal equation

The BOLD signal is related to deoxyhemoglobin content and blood volume via an equation that we term the BOLD signal equation. Recently Stephan et al. (2007) derived a BOLD signal equation for Balloon models which had superior performance to other BOLD signal equations on their comparison data. In the present notation this relation is

$$y = V_0\left[k_1\left(1-\frac{Q}{Q_0}\right)+k_2\left(1-\frac{Q\rho_f V_0}{Q_0\xi}\right)+k_3\left(1-\frac{\xi}{\rho_f V_0}\right)\right], \tag{16}$$

where V_0 is the equilibrium fractional blood volume content (i.e., the equilibrium value of V_f/V_v in the notation of Section 4), Q_0 is the equilibrium deoxyhemoglobin concentration, $\xi/\rho_f V_0$ is the dimensionless normalized blood volume (i.e., V_f/V_{f0} in the notation of Section 4), k_1,k_2,k_3 are the signal equation coefficients derived by Obata et al. (2004) whose estimation in the context of dynamic causal modelling was analyzed by Stephan et al. (2007).

8. Boundary conditions

To solve the set of hemodynamic equations derived in Sections 3–6 in real systems, appropriate boundary conditions must be specified, prescribing how blood enters and leaves the tissue. Separate inflow and outflow conditions are thus described in this section.

8.1. Inflow boundary condition

The neuronal signal Eq. (1) describes the scalar input flow modulation and this must be matched to the blood flow velocity field $\mathbf{v}$ at the boundary. As described in Section 1, when viewed from outside the cortical sheet the inflow arteries are well separated from one another and enter approximately perpendicular to the cortical sheet. Fig. 5 shows the assumed geometry of inflow region; i.e., we assume each inflow region has a cylindrical boundary with the cortical tissue and that blood flow is axially symmetric out of each inflow region.

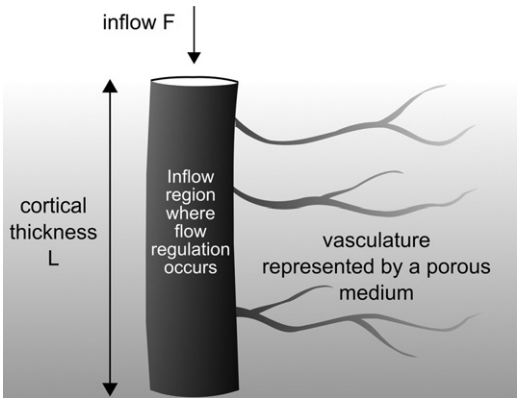

Fig. 5. Schematic showing blood inflow zone, a magnification of the boxed area in Fig. 1. Total blood inflow F into the cortex is shown. The approximately cylindrical blood inflow region forms the boundary to the poroelastic model. The geometric relationship between F, and v the blood velocity at the boundary, can be seen. The radius of the cylindrical inflow region is $r_{\mathbf{in}}$.

The local rate of blood volume inflow is given by

$$\frac{dV_f}{dt} = F, \tag{17}$$

where r_{in} is the radius of the inflow region, as shown in Fig. 5. Since the inflow must be equal to the flux out of the curved surface of the cylinder A_1, we have

$$\int_{A_1} \mathbf{v}\cdot d\mathbf{A} = F. \tag{18}$$

Assuming axial symmetry yields an equation relating the flow F in Eq. (1) to the blood flow velocity field $\mathbf{v}$; i.e.,

$$\mathbf{v} = F\frac{1}{2r_{\text{in}}L}\hat{\mathbf{r}}, \tag{19}$$

where $\hat{\mathbf{r}}$ is a unit radial vector pointing outwards that spreads the flow from the center of the inflow cylinder.

An alternative to specifying inflow via the above boundary condition is to specify inflow within an inflow region via the mass conservation Eq. (5). The mass conservation equation with source terms added is

$$\frac{\partial\xi}{\partial t} = -\rho_f\nabla\cdot\mathbf{v} + FH_{r_0}(\mathbf{r})\hat{\mathbf{r}}, \tag{20}$$

where the second term on the right hand side represents inflow that is spread the flow over the inflow region and where $H_{r_0}(\mathbf{r})$ is defined by

$$H_{r_0}(\mathbf{r}) = \frac{1}{\pi r_0^2}, \tag{21}$$

for $r \le r_0$, with $H_{r_0}(\mathbf{r}) = 0$ for $r > r_0$.

8.2. Outflow boundary condition

The outflow condition incorporates the physical process in which blood outflow occurs due to the higher blood pressure pushing blood into vessels downstream. Thus in our model the speed of blood outflow is proportional to the pressure difference between the outflow region and the ascending vein, and is assumed to be in a direction normal to the boundary of the outflow region. Hence,

$$v_{\text{out}} = c_3(P - P_V) \tag{22}$$

$$\approx c_3 P, \tag{23}$$

where c_3 is the proportionality constant and where Eq. (23) implicitly assumes that the blood pressure in the ascending vein

P_V can be neglected. As noted in Section 6, the zero reference point of pressure is atmospheric pressure. The neglect of P_V is justified by considering Lipowsky (2005) who provided experimental measure of pressure in rat cerebral microvasculature that showed a fourfold difference between arteriole and venule blood pressure. A similar pressure difference in human cerebral microvasculature would justify neglecting P_V relative to P in obtaining (23) from (22).

In the outflow region the blood flow is partially obstructed. We now demonstrate that the boundary condition (23) can be expressed in a form that shows it describes a partially obstructive barrier to the fluid and thus acts to inflate the vessels with blood. Near an output boundary where we define x along the normal to the outflow boundary the mass conservation Eq. (5) can be expressed as

$$\frac{\partial \xi}{\partial t} = -\rho_f \frac{\partial v_{\text{out}}}{\partial x}. \tag{24}$$

Using the outflow condition (23) yields

$$\frac{\partial \xi}{\partial t} = -c_3 \rho_f \frac{\partial P}{\partial x}. \tag{25}$$

Applying the constituent relation (15) then yields

$$\frac{\partial \xi}{\partial t} = -c_3 c_2 \rho_f \frac{\partial \xi^\beta}{\partial x}, \tag{26}$$

where c_2 is the proportionality constant in Eq. (15). Finally by approximating the right hand side of Eq. (26) to first order in ξ near the boundary, we find

$$c_3 c_2 \rho_f \beta \xi_0^{\beta-1} \frac{\partial \xi}{\partial x} + \frac{\partial \xi}{\partial t} = 0, \tag{27}$$

where ξ_0 is the equilibrium value of ξ. The boundary condition (27) mathematically describes a partially obstructing boundary (Higdon, 1986) which impedes the outflow of blood from the cortical tissue. Such an obstruction of blood outflow will lead to inflation of the cortical vasculature as inflow of blood will exceed outflow until the pressure rises in the cortical vasculature sufficiently to establish a balance. Thus our model predicts inflation of the cortical vasculature, the basis of Balloon model approximations. It should be noted the present outflow condition is slightly different from the corresponding Balloon model outflow condition: here outflow is dictated by the pressure near the outflow point, whereas in the Balloon model it is the pressure in the balloon (i.e., an average pressure over a region of brain) that dictates the outflow. We discuss this point further in the next section where we show they are equivalent under certain conditions.

Further insight into the behavior at the boundary can be established by comparing with a mathematically equivalent but physically quite distinct example of this type of boundary condition. Higdon (1986) considered optical reflection and showed that in two dimensions a perfectly absorbing boundary condition for an optical wave ξ propagating with speed v at an angle α to the normal to a right boundary is given by

$$v\cos\alpha \frac{\partial \xi}{\partial x} + \frac{\partial \xi}{\partial t} = 0. \tag{28}$$

Waves propagating with angles different from α at a boundary condition (28) are partially reflected (the hemodynamic analog is partial obstruction of outflow) and the extent of reflection of the wave at the boundary depends only on $\cos\alpha$. The mathematical equivalence with our model can now be established. For our boundary condition (27), the disturbance in ξ propagates normal to the outflow boundary. Comparison of (27) and (28) shows that by analogy to the optical case, ξ is partially obstructed at the boundary. The extent of obstruction depends only on the product $c_3 c_2 \rho_f \beta \xi_0^{\beta-1}$ ($\cos\alpha$ in the optical case). Obstruction will be perfect in the physiologically unrealistic case $c_3 c_2 \rho_f \beta \xi_0^{\beta-1} \to 0$, implying that either $c_2 \to 0$ or $c_3 \to 0$. Note that $c_2 \to 0$ corresponds to the unphysical case of perfectly rigid brain tissue and $c_3 \to 0$ to brain tissue without outflow vessels.

9. Poroelastic temporal dynamics and the Balloon model as a limiting case

In this section we demonstrate that our spatiotemporal model reproduces a widely used Balloon model in an appropriate limit. By showing this correspondence we clarify the conditions for validity of this Balloon model (and thus of other similar ones, at least approximately), and also clarify implicit assumptions underlying such models. Our demonstration of the correspondence between the present model and a Balloon model immediately implies that our model can at least reproduce all experimentally verified successes of this Balloon model, including the major temporal characteristics of observed hemodynamic responses.

The specific Balloon model which we demonstrate to be reproduced by our model in the appropriate limit is the Friston et al. (2003) model (hereafter simply referred to as the Balloon model), whose temporal properties have previously been analytically investigated in detail (e.g., Robinson et al., 2006). A similar approach would clarify the relationships of our spatiotemporal model to other Balloon models.

In order to show that our model reproduces the Balloon model, the following simplifying assumptions must be made, and the following limits taken: (i) The BOLD response is averaged over the entire voxel and each voxel is independent and fixed in size. (ii) One blood inflow and one blood outflow point exist for each voxel. (iii) The vasculature can be unrolled into a linear tube without disturbing the predicted hemodynamic response within a voxel. (iv) The Balloon model neuronal activity z_B (called z by Friston et al., 2003) is the total neuronal activity in the voxel. (v) The characteristic time for neuronal flow modulation is longer than the blood transit time through the voxel. Fig. 6 shows a schematic representation of the vasculature, as approximated in the Balloon model.

In the following subsections we show that the present model reproduces the Balloon model in the appropriate limit. Our model equations do not have a one to one correspondence with those of the Friston et al. (2003) model; rather, we show that the Balloon model is reproduced by taking appropriate limits and performing changes of variables into the notation of Friston et al. (2003). The state variables of the Balloon model are normalized total or average quantities for a voxel and are suffixed B for Balloon below to clearly distinguish them from the dimensional variables of the present model. In the following subsections the volume element

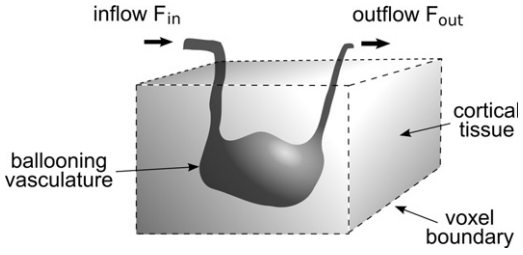

Fig. 6. Schematic of the balloon within a voxel assumed in balloon models. The major structural features are shown including blood inflow, CBV content within the balloon, and blood outflow. The vasculature is assumed to be able to be unrolled into to a linear tube without disturbing the predicted hemodynamic response. The balloon is approximated as a single unit to allow blood within it is be approximated as well mixed.

under consideration in our model will be the voxel, in accord with the Balloon model assumption (i) above.

9.1. Neuronal signal

Two equations of the Friston et al. (2003) model describe neuronal signalling and can be reproduced from the neuronal Eq. (1). Friston et al. (2003) defined F_B to be a normalized blood volume inflow

$$F_B = F/F_0, \tag{29}$$

where F_0 is the equilibrium flow. Furthermore they defined s_B implicitly via

$$\frac{dF_B(t)}{dt} = s_B(t). \tag{30}$$

Substituting both these relations into Eq. (1) and dividing by F_0 yields

$$\frac{ds_B}{dt} + \kappa s_B + \gamma(F_B - 1) = \frac{1}{F_0}\int h(z,\mathbf{r})\,dr, \tag{31}$$

where the integral on the right hand side sums neuronal activity in the voxel. The Balloon model activity z_B of Friston et al. (2003) is the total activity within a voxel divided by F_0,

$$z_B = \frac{1}{F_0}\int h(z,\mathbf{r})\,dr. \tag{32}$$

Eqs. (31) and (32) then yield

$$\frac{ds_B}{dt} = z_B - \kappa s_B - \gamma(F_B - 1). \tag{33}$$

Eqs. (30) and (33) are exactly the first two Balloon model equations of Friston et al. (2003).

9.2. Blood volume evolution

The Balloon model contains an equation governing the evolution of blood volume on a voxel. We now show that this is reproduced by the present model, in the appropriate limit, by combining the mass conservation Eq. (4), the constituent Eq. (15), and the output boundary condition (23).

At the output boundary, the outflow is dependent on the vascular pressure given by Eq. (23). Using the constituent relation (15) the blood outflow is then given by

$$F_{\text{out}} = c_3\int_{\text{outflow}} c_2\xi^\beta dA, \tag{34}$$

where F_{out} is the integral over the outflow surface. Now considering mass conservation and applying Gauss's theorem to Eq. (5) over the entire vascular volume V_v within the voxel yields

$$\int_{V_v}\frac{\partial\xi}{\partial t}\,dV_e = -\int_{\partial V_v}\rho_f\mathbf{v}\cdot d\mathbf{A}, \tag{35}$$

where V_v is the voxel under consideration. Interchanging the order of integration and differentiation on the left hand side of (35) then yields

$$\rho_f\frac{dV_f}{dt} = -\rho_f\int_{\text{surface}}\mathbf{v}\cdot d\mathbf{A}, \tag{36}$$

where V_f is the blood volume in the voxel. Splitting the right hand side surface integral into inflowing and outflowing flux zones then yields

$$\frac{dV_f}{dt} = F_{\text{in}} - F_{\text{out}}, \tag{37}$$

where F_{in} and F_{out} are the total blood volume inflow and outflow, respectively. Substituting Eq. (34) into Eq. (37) then gives

$$\frac{dV_f}{dt} = F_{\text{in}} - c_2c_3\int_{\text{outflow}}\xi^\beta\,dA, \tag{38}$$

where $\hat{\mathbf{n}}$ is the outward pointing normal vector to the surface $\mathbf{A}$. Friston et al. (2003) defined the Balloon model state variable v_B to be the normalized volume

$$v_B = V_f/v_0, \tag{39}$$

where v_0 is the equilibrium cerebral blood volume in the voxel and inflow to be given as given by Eq. (29). The hemodynamic transit time

$$\tau = v_0/F_0, \tag{40}$$

is the characteristic time taken for a voxel to refill. Substituting F_B into Eq. (38) and dividing by F_0 yields

$$\tau\frac{dv_B}{dt} = F_B - \frac{c_2c_3}{F_0}\int_{\text{outflow}}\xi^\beta\,dA. \tag{41}$$

The second term on the right hand side can be expressed in a normalized form by noting that at equilibrium Eq. (41) yields the following relation between steady state parameters:

$$F_0 = c_2c_3\overline{\xi}_0^2A_{\text{out}}, \tag{42}$$

where $\overline{\xi}_0$ is the equilibrium blood mass content per unit volume averaged over the outflow area and A_{out} is the total area of the ouflow surface. Thus Eq. (41) can be expressed as

$$\tau\frac{dv_B}{dt} = F_B - \frac{\overline{\xi^\beta}}{\overline{\xi}_0^\beta}, \tag{43}$$

where $\overline{\xi}$ is the blood mass content per unit volume averaged over the outflow area.

We now consider the second term on the right hand side which is the normalized outflow from the voxel. In our case the term is proportional to the normalized ξ^β averaged over the outflow area. In the Balloon Model the outflow term is proportional to $v_B^{1/\alpha}$. We next show the two are the same in the appropriate limit.

As mentioned earlier β has not been measured *in situ*, nonetheless we may identify $\beta = 1/\alpha$ linking the small scale mechanical properties of vasculature described by β with the definition of α measured and derived by Grubb et al. (1974) from the steady state relation between flow and volume. Experimentally β is known to satisfy $1 \le \beta \le 5$ (Fung, 1993) and $\alpha \approx 0.32$ (Friston et al., 2003) so that this identification is consistent with experimental measures ($\alpha \approx 0.32$ corresponds to $\beta \approx 3.1$). This identification makes explicit the connections between microscopic mechanical properties and macroscopic properties which were implicit in work such as that of Grubb et al. (1974) and Mandeville et al. (1999).

Naively it might be assumed that, since pressure would be uniform inside the balloon, the term in Eq. (38) would be proportional $v_B^{1/\alpha}$ and in the Balloon limit the equations would correspond directly. Unfortunately, this is inadequate since it is generally not the case that our model has uniform pressure within the vascular volume. Hence, for the vasculature to reproduce balloon behavior, the neuronal flow modulation characteristic time must be longer than the blood transit time so that modulations in ξ are slowly varying; experimental measures by Buxton et al. (1998) suggest it is a factor of ~ 2 longer. In this case, the vasculature will tend to inflate approximately as a single unit without fine spatial structure in ξ thus ensuring the normalized $\overline{\xi^\beta}$ (with average evaluated over the outflow surface) is proportional to $v_B^{1/\alpha}$. Thus we may identify the normalized

outflow as

$$f_{\text{out}} \propto v_B^{1/\alpha}, \tag{44}$$

so the latter right hand side term of Eq. (38) will be proportional to $v^{1/\alpha}$, and the volume relation given by

$$\tau \frac{dv_B}{dt} = F_B - v_B^{1/\alpha}, \tag{45}$$

is reproduced.

9.3. Hemoglobin dynamics

The deoxyhemoglobin equation of the Balloon model is reproduced by the present model in the appropriate limit which we now show. The deoxyhemoglobin equation of the Balloon model was adopted directly from the Buxton and Frank (1997) model. Before proceeding, we note that in our model conversion of oHB to dHB is proportional to oHB concentration, similarly to Buxton and Frank (1997), except that they spatially aggregated its effects by integrating along blood vessels. Nonetheless the two models differ in an essential way: in the present model the BOLD signal arises from dHB in the single vascular compartment (i.e., from both capillaries and veins), while in the Balloon model it is assumed that the BOLD signal arises only from the venous balloon. In order to reduce the present model to the Balloon model we will further impose the Balloon model assumptions that all deoxygenation occurs in the capillary bed whence the blood flows into the venous balloon where BOLD signal arises.

The rate of change of the Q in a voxel can be found by integrating Eq. (13) over the interior vascular volume V_v and applying Gauss's theorem, which yields

$$\int_{V_v} \frac{\partial Q}{\partial t} dV_e = -\int_{\partial V_v} Q\mathbf{v} \cdot d\mathbf{A} + \int_{V_v} (\psi\xi - Q)\eta \, dV_e, \tag{46}$$

which can be simplified by evaluating the first integral and spitting the second integral into averaged flows in and out of the voxel, to yield

$$\frac{dq}{dt} = Q_{\text{in}}F_{\text{in}} - Q_{\text{out}}F_{\text{out}} + \int_{V_v} (\psi\xi - Q)\eta \, dV_e, \tag{47}$$

where q is the deoxyhemoglobin content within the voxel (whereas upper case Q s denote concentrations). The first and third terms on the right hand are the inflow of Q and consumption of Q within the voxel. In order to assume all deoxygenation occurs in the capillary bed we must determine an expression for the dHB content after the blood exits the capillary bed. For a capillary bed with input flow F and no deoxygenated hemoglobin at the inflow point, Buxton and Frank (1997) showed that the deoxygenated hemoglobin flux leaving the capillary bed is given by

$$FQ = FC_A E(F_B, \rho), \tag{48}$$

where C_A is the arterial oxygen concentration and $E(F_B,\rho)$ is defined by them as the net extraction of oxygen (i.e., the fraction of oxygen extracted after the blood passes through the capillary bed). The first and third right hand side terms of Eq. (47) may be replaced by the right hand side of Eq. (48) and, by further adopting the Buxton and Frank (1997) approximation of a well mixed venous balloon, we obtain

$$\frac{dq}{dt} = FC_A E(F_B, \rho) - Q_{\text{out}}F_{\text{out}}. \tag{49}$$

Buxton and Frank (1997) showed that C_A can be expressed in terms of the steady state parameters as

$$C_A = q_0/(v_0\rho_0), \tag{50}$$

where q_0 is the equilibrium deoxyhemoglobin content, v_0 the equilibrium blood volume in the voxel and ρ_0 is the equilibrium oxygen extraction fraction (i.e., the equilibrium fraction of oxygen extracted after the blood passes through the capillary bed). Thus Eq. (49) can be expressed as

$$\frac{dq}{dt} = F\frac{q_0}{v_0\rho_0}E(F_B,\rho) - Q_{\text{out}}F_{\text{out}}. \tag{51}$$

Buxton et al. (1998) assumed that the balloon was well mixed so that the outflowing deoxyhemoglobin concentration equalled the average concentration i.e. the total hemoglobin content of the voxel dividing by the blood volume within the voxel:

$$Q_{\text{out}} = q/(v_0 v_B). \tag{52}$$

Friston et al. (2003) expressed their results in terms of a normalized deoxyhemoglobin content of the voxel

$$q_B = q/q_0. \tag{53}$$

Expressing Eq. (51) in terms of q_B, F_B, and v_B, and applying Eq. (52) for the outflowing Q yields

$$q_0\frac{dq_B}{dt} = F_0F_B\frac{q_0}{v_0\rho_0}E(F_B,\rho) - \frac{q_0q_B}{v_0v_B}F_0f_{\text{out}}, \tag{54}$$

whence using Eq. (40) for τ and Eq. (44) for f_{out} yields

$$\tau\frac{dq_B}{dt} = \frac{F_BE(F_B,\rho)}{\rho_0} - \frac{q_Bv_B^{1/\alpha}}{v_B}, \tag{55}$$

which is the final Balloon model equation of Friston et al. (2003).

10. Summary and discussion

We have developed a spatiotemporal poroelastic hemodynamic model for use in BOLD signal analysis and fMRI, to establish a quantitative physiologically based foundation for understanding hemodynamic responses, making new predictions for comparison with experiment, and for calculating quantities such as the hemodynamic response function and improved priors for statistical analyses (e.g., in dynamic causal modelling).

The main results are:

(a) The spatiotemporal hemodynamic model developed incorporates the physical principles of mass conservation, force balance, total hemoglobin conservation, and neuronal flow regulation. The main governing equations are Eqs. (1), (5), (13) and (14). Together with Eqs. (15) and (16) these constitute a closed set of hemodynamic equations that will enable the hemodynamic response to given neural activity to be obtained by applying standard methods for solving fluid dynamics equations of this broad class.

(b) The present model gives a description of hemodynamic response that is independent of instrumental features such as voxel size. Since voxel sizes are decreasing with advances in technology, hemodynamic coupling between voxels is becoming a significant issue. Hence, our hemodynamic theory, which is independent of measurement apparatus, provides an essential foundation for understanding observed spatial hemodynamic responses. Further our spatiotemporal model can describe the coupling between adjacent voxels and can thus provide mutual constraints on their BOLD signals for use in fMRI.

(c) The model predicts cortical vessel inflation in regions where neuronal activity increases. This occurs due to an increase in blood content that cannot exit from the cortical vasculature at a rate equal to its inflow. In the present model this arises from the fact that the outflow rate of blood is proportional to the blood pressure difference between capillaries and venules, and ascending veins, leading to a partially obstructing

boundary condition. Thus the central approximation of Balloon models (i.e. the ballooning of the vasculature) is predicted and elucidated as a consequence of the physiological properties incorporated in the present model.

(d) Our model directly includes both the spatial and temporal aspects of BOLD, in contrast to prior Balloon models, which described only temporal aspects of the BOLD response. Further, the poroelastic model reproduces the Friston et al. (2003) Balloon model in the appropriate limit.

(e) The poroelastic model clarifies many of the assumptions of Balloon models and thus quantifies the regimes of validity of Balloon models. The assumptions which are required to reproduce a Balloon model from the present model are (see Section 9 for more details): (i) The BOLD response is averaged over the entire voxel and each voxel is independent and fixed in size. (ii) One blood inflow and one blood outflow point exist for each voxel. (iii) The vasculature can be unrolled into a linear tube without disturbing the predicted hemodynamic response within a voxel. (iv) The Balloon model neuronal activity z_B (called z by Friston et al., 2003) is the total neuronal activity in the voxel. (v) The characteristic time for neuronal flow modulation is longer than the blood transit time through the voxel. Assumptions (i)–(iv) are expressed or strongly implied in the existing literature on Balloon models, but we have not found any discussion of (v) in the literature. However in relation to (v), we note most studies suggest there is an upper bound of about 2 s on the transit time. Given the prevalence of slow oscillations (periods >10 s) in resting state hemodynamics it is likely that the characteristic time for neuronal flow modulation is longer than blood transit time, under physiological conditions. Balloon models have been successful in describing hemodynamic response when voxel sizes are moderately large. In order to model the spatial aspects of BOLD these restrictive assumptions must be relaxed when voxel sizes are sufficiently small that voxels become interdependent.

(f) The present model reproduces the Friston et al. (2003) Balloon model as a limiting case. Hence it can immediately reproduce *at least* the range of phenomena explained by that earlier model, including the main features of the temporal dynamics of BOLD.

In summary, the model developed here is closely based on known physiological and anatomical properties of cortical tissue and vasculature and is expressed in terms of blood velocities, forces, and elastic properties. Hence, it clarifies how relations such as the Grubb relation (44) relate to assumptions about the underlying physiological properties of the system. Experimental literature describing cerebral blood flow and volume tends to relate these quantities in an averaged sense, but rarely are these described in terms of tissue properties. As spatial properties of BOLD response are investigated in increasing detail in the future, measures of CBF and CBV may provide insights into mechanisms and structures, especially when combined with interpretations via modelling. Further, different measurement techniques average CBV and CBF in different ways and the model can help us understand averaging implicit in observations, e.g., by implementing equivalent averaging in the model and comparing these results with observations.

Overall, the present model thus provides a basis for further analysis, applications, and for making new predictions for comparison with experiment. For example it can be coupled to neural activity to allow the derivation of a spatiotemporal HRF. Such an HRF and its properties will be published in future work, along with comparison with experimental high spatial resolution BOLD measurements. Since spatial and temporal responses are intimately connected, the model will also provide further constraints and priors for empirical inverse modeling of BOLD responses so that signal to noise ratios can be improved in high spatial resolution fMRI. The present model could also be extended to explicitly include a third spatial dimension (cortical depth and layering) and refinements such as delayed compliance and multiple compartments.

Acknowledgements

The authors thank Robert Turner, Peter Dayan, and Mark Schira for stimulating discussions. The Australian Research Council supported this work.

References

Acheson, D.J., 1990. Elementary Fluid Dynamics. Oxford Press, Oxford, p. 4.
Bennett, M.R., Farnell, L., Gibson, W.G., 2007. Origins of blood volume change due to glutamatergic synaptic activity at astrocytes abutting on arteriolar smooth muscle cells. J. Theor. Bio. 250, 172–185.
Barash, B.F.C., Stoelting, R.K., Cahalan, M., Stock, C., 2009. Clinical Anesthesia. Lippincott Williams and Wilkins, Philadelphia.
Bear, J., 1972. Dynamics of Fluids in Porous Media. Elsevier, Amsterdam.
Buxton, R.B., Frank, L.R., 1997. A model for the coupling between cerebral blood flow and oxygen metabolism during neural stimulation. J. Cereb. Blood Flow Metab. 17, 64–72.
Buxton, R.B., Wong, E.C., Frank, L.R., 1998. Dynamics of blood flow and oxygenation changes during brain activation: the Balloon model. Magn. Reson. Med. 39, 855–864.
Conrad, B., Klingelhöfer, J., 1989. Dynamics of regional cerebral blood flow for various visual stimuli. Exp. Brain Res. 77, 437–441.
Damoiseaux, J.S., Rombouts, S.A.R.B., Barkhof, F., Scheltens, P., Stam, C.J., Smith, S.M., Beckmann, C.F., 2006. Consistent resting state networks across healthy subjects. Proc. Natl. Acad. Sci. 103, 13848–13853.
Darcy, H., 1856. Les Fontaines Publiques de la Ville de Dijon. Dalmont, Paris.
Duvernoy, H.M., Vannson, J.L., 1981. Cortical blood vessels of the human brain. Brain Res. Bull. 7, 519–579.
Fox, M.D., Raichle, M.E., 2007. Spontaneous fluctuations in brain activity observed with functional magnetic resonance imaging. Nat. Rev. Neurosci. 8, 700–711.
Friston, K.J., 1995. Regulation of rCBF by diffusible signals: an analysis of constraints on diffusion and elimination. Hum. Brain Mapp. 3, 56–65.
Friston, K.J., Mechelli, A., Turner, R., Price, C.J., 2000. Nonlinear responses in fMRI: the Balloon model, Volterra Kernels, and other hemodynamics. NeuroImage 12, 466–477.
Friston, K.J., Harrison, L., Penny, W., 2003. Dynamic causal modelling. NeuroImage 19, 1273–1302.
Fung, Y.C., 1993. Biomechanics: Mechanical Properties of Living Tissues. Springer, New York.
Griffiths, D.J., 1989. Introduction to Electrodynamics. Prentice-Hall, London, p. 71.
Grubb, R.L., Raichle, M.E., Eichling, J.O., Ter-Pogossian, M.M., 1974. The effects of changes in Pa CO_2 on cerebral blood volume, blood flow, and vascular mean transit time. Stroke 5, 630–639.
Harrison, R.V., Harel, N., Panesar, J., Mount, R.J., 2002. Blood capillary distribution correlates with hemodynamic-based functional imaging in cerebral cortex. Cereb. Cortex 12, 225–233.
Haydon, P.G., Carmignoto, G., 2006. Astrocyte control of synaptic transmission and neurovascular coupling. Physiol. Rev., 1009–1031.
Higdon, R.L., 1986. Absorbing boundary conditions for difference approximations to the multi-dimensional wave equation. Math. Comput. 47, 437–459.
Hoffbrand, A.V., Petit, J.E., Moss, P.A.H., 2004. Essential Haematology, fourth ed. Blackwell Science, Hong Kong.
Kong, Y., Zheng, Y., Johnston, D., Martindale, J., Jones, J., Billings, S., Mayhew, J., 2004. A model of the dynamic relationship between blood flow and volume changes during brain activation. J. Cereb. Blood Flow Metab. 24, 1382–1392.
Lipowsky, H.H., 2005. Microvascular rheology and hemodynamics. Microcirculation 12, 5–15.
Logothetis, N.K., Pauls, J., Augath, M., Trinath, T., Oeltermann, A., 2001. Neurophysiological investigation of the basis of the fMRI signal. Nature 412, 150–157.
Long, C.J., Brown, E.N., Triantafyllou, C., Aharon, I., Wald, L.L., Solo, V., 2005. Nonstationary noise estimation in functional MRI. NeuroImage 28, 890–903.
Lund, T.E., Madsen, K.H., Sidaros, K., W.-L, .Luo, Nichols, T.E., 2005. Non-white noise in fMRI: does modelling have an impact. NeuroImage 29, 54–66.
Mandeville, J.B., Marota, J.J.A., Ayata, C., Zaharchuk, G., Moskowitz, M.A., Rosen, B.R., Wiesskoff, R.M., 1999. Evidence of cerebrovascular postarteriole windkessel with delayed compliance. J. Cereb. Blood Flow Metab. 19, 679–689.
Nair, D.G., 2005. About being BOLD. Brain Res. Rev. 50, 229–243.
Obata, T., Liu, T., Miller, K.L., Luh, W., Wong, E.C., Frank, L.R., Buxton, R.B., 2004. Discrepancies between BOLD and flow dynamics in primary and supplementary motor areas: application of the balloon model to the interpretation of BOLD transients. NeuroImage 21, 144–153.

Poiseuille, J.L.M., 1846. Recherches expérimentales sur le mouvement des liquides dans les tubes de très-petits diamètres. In: Mémoires presentés par divers savants à l'Academie Royale des Sciences de l'Institut de France, vol. IX, pp. 433–544.
Raichle, M.E., MacLeod, M.A., Snyder, A.Z., Powers, W.J., Gusnard, D.A., Shulman, G.L., 2001. A default mode of brain function. Proc. Natl. Acad. Sci. 98, 676–682.
Reira, J.J., Wan, X., Jimenez, J.C., Kawashima, R., 2006. Nonlinear local electrovascular coupling 1: a theoretical model. Hum. Brain Mapp. 27, 896–914.
Robinson, P.A., Drysdale, P.M., Van der Merwe, H., Kyriakou, E., Rigozzi, M., Germanoska, B., Rennie, C.J., 2006. BOLD responses to stimuli: dependence on frequency, stimulus form, amplitude, and repetition rate. NeuroImage 31, 585–599.
Shmuel, A., Augath, M., Oeltermann, A., Logothetis, N.K., 2006. Negative functional MRI response correlates with decreases in neuronal activity in monkey visual area V1. Nat. Neurosci. 9, 569–577.
Smirnakis, S.M., Schmid, M.C., Weber, B., Tolias, A.S., Augath, M., Logothetis, N.K., 2007. Spatial specificity of BOLD versus cerebral blood volume fMRI for mapping cortical organisation. J. Cereb. Blood Flow Metab. 27, 1248–1261.
Stephan, K.E., Weiskopf, N., Drysdale, P.M., Robinson, P.A., Friston, K.J., 2007. Comparing hemodynamic models with D.C.M. NeuroImage 38, 387–401.
Turner, R., Thomas, D., 2006. How can cerebral blood volume change? Presented at the 12th International Conference of Functional Mapping of the Human Brain, June 11–15, 2006, Florence, Italy. NeuroImage, vol. 31, Supplement 1.
Vanzetta, I., Hildsheim, R., Grinvald, A., 2005. Compartment-resolved imaging of activity-dependent dynamics of cortical blood volume and oximetry. J. Neurosci. 25, 2233–2244.
Wang, H., 2000. Theory of Linear Poroelasticity with Applications for Geomechanics and Hydrogeology. Princeton University Press, Princeton, NJ.
Zonta, M., Angulo, M.C., Gobbo, S., Rosengarten, B., Hossmann, K.A., Pozzan, T., Carmignoto, G., 2003. Neuron-to-astrocyte signalling is central to the dynamic control of brain microcirculation. Nat. Neurosci. 6, 43–50.
Zheng, Y., Johnston, D., Berwick, J., Chen, D., Billings, S., Mayhew, J., 2005. A three-compartment model of the hemodynamic response and oxygen delivery to the brain. NeuroImage 28, 925–939.